Experimental Nonlinear Modal Analysis of an F-16 Aircraft using Phase-locked Loop Control

Tong Zhou * and Ghislain Raze †
University of Liege, Liege, 4000, Belgium

Giancarlo Kosova ‡
University of Liege, Liege, 4000, Belgium
Siemens Digital Industries Software, Leuven, 3001, Belgium

Gaëtan Kerschen§
University of Liege, Liege, 4000, Belgium

This study leverages phase-locked loop (PLL) control and adaptive filtering for the experimental identification of the nonlinear modal parameters of an F-16 aircraft. Specifically, PLL effectively tracks the backbones of three aircraft modes, enabling the extraction of resonance frequencies, mode shapes, and damping ratios, all of which vary with vibration amplitude. Additionally, the nonlinear frequency responses of 3:1 superharmonic resonances are identified. The results reveal that the F-16 aircraft exhibits softening effects due to joint friction in the wing-to-payload connections, as well as clearance-induced nonlinearity. The onset of contact is further illustrated through time-harmonic analysis of modal deflection shapes.

Nomenclature

a	=	modal amplitude
A	=	harmonic response amplitude
$\mathbf{C}$	=	linear damping matrix
F	=	point force amplitude
$\mathbf{F}$	=	excitation force vector
$\mathbf{F}_{\text{NL}}$	=	nonlinear restoring force vector
K_P	=	proportional gain of the controller
K_I	=	integral gain of the controller
$\mathbf{K}$	=	linear stiffness matrix
$\mathbf{M}$	=	system mass matrix

*Postdoc Fellow, Department of Aerospace and Mechanical Engineering, zhoutong01993@gmail.com (corresponding author).
†Postdoc Fellow, Department of Aerospace and Mechanical Engineering, G.Raze@uliege.be.
‡Ph.D. candidate, Department of Aerospace and Mechanical Engineering, giancarlo.kosova@siemens.com
§Full Professor, Department of Aerospace and Mechanical Engineering, g.kerschen@uliege.be.

P = excitation power input

$\mathbf{Q}$ = basis vector containing harmonic functions

t = time

T = the minimum period of a nonlinear normal mode motion

U = voltage fed to the shaker

$\ddot{x}$ = point acceleration response

$\mathbf{x}$ = system displacement vector

z_s, z_c = Fourier coefficients for sine and cosine functions

$\mathbf{z}$ = Fourier coefficients vector

$\Delta\varphi$ = instant phase lag difference

θ = instant forcing phase

κ = harmonic number

μ = adaptive filter gain

ξ = damping ratio

$\mathbf{\Phi}$ = mode shape

φ = phase lag between acceleration and excitation

ω = the angular frequency of excitation

I. Introduction

Ground vibration testing (GVT) has become a standard procedure in aircraft development and certification [1, 2]. A key objective of GVT is to identify the modal parameters of the tested aircraft, providing essential data for validating or refining finite element models. These models are then used to predict flutter margins during flight tests and to detect potential aeroelastic issues [3]. Additionally, GVT plays a crucial role in ensuring the safety and reliability of spacecraft and rockets during actual launch operations [4].

Modal identification and analysis are essential in experimental vibration testing. Advanced commercial software packages such as Siemens Testlab and Brüel & Kjaer BK Connect are widely used in industry, operating under the fundamental assumption of linear dynamic behavior. In this framework, modal parameters, namely mode shapes, resonance frequencies, and damping ratios, remain invariant with respect to vibration amplitude, and frequency response functions (FRFs) can be directly synthesized using modal superposition. However, as aerospace structures are pushed to expand their performance envelope, nonlinear behaviors are increasingly observed during experimental testing of modern flight vehicles and their subassemblies [5]. Common manifestations of nonlinearity include frequency-energy dependence in resonance behavior (e.g., softening and hardening effects), jump phenomena between coexisting vibration

states, the emergence of rich harmonic content, and nonlinear modal interactions [6]. These effects present significant challenges in establishing a systematic experimental testing procedure for the dynamic characterization of nonlinear systems.

In this context, the nonlinear normal mode (NNM) theory offers a valuable and solid theoretical framework for interpreting a wide range of nonlinear dynamical phenomena. The NNMs, defined either as periodic motions of a conservative system [7, 8] or as invariant manifolds [9–11], represent a generalization of the mode concept to nonlinear systems. The analysis of NNMs is particularly useful for studying vibrational responses near resonance across various excitation levels. Similar to phase resonance in linear modal testing, a widely used experimental approach for identifying NNMs and their modal parameters primarily aims to isolate a specific NNM. This process relies on the so-called force appropriation [12], wherein the external forcing balances the dissipative forces inside the structure. This can be realized with a multi-point, multi-harmonic forcing, with each harmonic in phase quadrature with their collocated counterpart in the structural response [13–16]. To characterize the amplitude dependence of modal properties, one can either perform force appropriation at different force levels or suddenly stop the excitation and record free-decay data. However, in view of the associated practical difficulties, nonlinear force appropriation is most often performed with a single exciter applying monoharmonic forcing.

Recently, phase-locked loop (PLL) testing has been introduced as a more robust and effective alternative for identifying the NNMs of mechanical systems [17–19]. PLL testing utilizes an online phase detection module and controls the applied harmonic excitation through a feedback loop. In particular, a specific phase lag between the displacement and the forcing can be directly imposed through an automatic adjustment of the excitation frequency. PLL stands out as a model-free testing method, requiring limited information about the considered system. Nonetheless, an important assumption behind PLL is that the phase lag presents a monotonic behavior in the vicinity of the targeted resonance. Recent works have evidenced that PLL is a powerful method for identifying nonlinear modes of thin structures featuring geometric nonlinearity [18] and joint friction [20]. It is also suitable for dealing with nonlinear systems with variable or uncertain properties [19, 21]. Additionally, PLL testing can be adapted for identifying nonlinear frequency responses that contain crucial information about instabilities and bifurcations [18]; it can also provide valuable insights when nonlinear modal interactions are present [22, 23].

Despite significant progress, to the best of our knowledge, only one attempt has been made to identify the nonlinear modes of a real-world engineering structure using PLL testing [24]. These systems are often composed of structural components with joints and interfaces, introducing complex localized nonlinearities involving friction and contact [2, 25]. Demonstrating the advantages of the NNM framework—particularly PLL testing—in this context is highly valuable and represents a key objective of this study. To this end, we focus on the experimental identification of wing bending and torsion modes of a full-scale F-16 aircraft. Our nonlinear modal analysis is based on PLL feedback control with adaptive filtering. To detect and characterize nonlinearities in the F-16 aircraft, we employ a modified

restoring force surface method combined with modal deflection shape analysis. Finally, adaptive filtering also allows the identification of 3:1 superharmonic resonances in the second and third wing torsional modes, a distinctive feature of nonlinear dynamical systems.

This paper is organized as follows. Section 2 introduces the fundamental principles of NNM identification using PLL testing. Section 3 provides an overview of the F-16 aircraft and the experimental setup. In Section 4, following the presentation of linear modal testing results, the experimental identification of nonlinear modes is performed, along with an analysis of their modal properties. Finally, conclusions are presented in Section 5.

II. Nonlinear Mode Identification using Phase-Locked Loop Control

NNM identification through force appropriation and its realization using PLL testing are discussed in this Section. A harmonically-excited nonlinear dynamical system is considered:

$$\mathbf{M}\ddot{\mathbf{x}}(t) + \mathbf{C}\dot{\mathbf{x}}(t) + \mathbf{K}\mathbf{x}(t) + \mathbf{F}_{\mathrm{NL}}\left(\mathbf{x}(t), \dot{\mathbf{x}}(t)\right) = \mathbf{F}(\omega, t), \tag{1}$$

where $\mathbf{M}$, $\mathbf{C}$ and $\mathbf{K}$ are the linear mass, damping and stiffness matrices, respectively. $\mathbf{x}(t)$ is the displacement vector and an overdot represents a time derivative. $\mathbf{F}_{\mathrm{NL}}\left(\mathbf{x}(t), \dot{\mathbf{x}}(t)\right)$ is the vector collecting nonlinear restoring forces and $\mathbf{F}(\omega, t)$ is the excitation force vector, with ω the angular frequency of excitation.

The objective of nonlinear mode identification is to determine the periodic motions of the underlying unforced, undamped system

$$\mathbf{M}\ddot{\mathbf{x}}(t) + \mathbf{K}\mathbf{x}(t) + \mathbf{F}_{\mathrm{NL,c}}\left(\mathbf{x}(t)\right) = \mathbf{0}, \quad \text{with } \mathbf{x}(t) = \mathbf{x}(t+T) \tag{2}$$

where $\mathbf{F}_{\mathrm{NL,c}}\left(\mathbf{x}(t)\right)$ is the conservative part of the nonlinear forces, and T is the minimum period of a NNM motion. The nonlinear modes and natural frequencies are known to have a dependence on vibrational energy [8, 26]; they resemble linear modal parameters when nonlinear effects are negligible. Another important quantity in nonlinear modal testing is a nonlinear frequency response curve (NFRC). Similar to the frequency response function (FRF) of a linear system, a NFRC represents a branch of periodic responses of the forced, damped system, i.e., a periodic solution to Eq. (1). The locus of phase quadrature points in a NFRC [27] is commonly referred to as the backbone curve, which illustrates the relationship between NNMs and NFRCs.

NNM force appropriation aims at determining the appropriate forcing $\mathbf{F}(\omega, t)$ to isolate a single nonlinear mode. This realization often hinges on satisfying phase quadrature conditions for which the dissipative forces balance out the excitation forces. In practice, nonlinear mechanical systems often feature well-separated modes, with the system response at a certain frequency primarily dominated by a single mode. In such cases, it has been demonstrated that

applying a single-point force comprising a single harmonic can achieve a satisfactory mode isolation [13, 18].

PLL testing has emerged as a promising model-free approach for identifying NNMs by exploiting the unique phase evolution property of nonlinear mechanical systems. It provides an automatic and reliable single-point force appropriation for isolating a nonlinear mode without needing a detailed system model, making it effective for studying complex nonlinear behavior. The key ingredient of PLL relies on the utilization of an excitation force controlled by a feedback loop through a specified set of force amplitude $\hat{F}$ and target phase lag $\hat{\varphi}$,

$$F_d(\hat{\varphi}, \hat{F}, t) = \hat{F} \sin\left[\theta(t)\right] = \hat{F} \sin\left[\int_0^t \omega(\tau)\mathrm{d}\tau\right], \tag{3}$$

with

$$\omega(t) = \hat{\omega}_o + K_P \Delta\varphi(t) + K_I \int_0^t \left[\Delta\varphi(\tau)\right] \mathrm{d}\tau. \tag{4}$$

Here, the forcing frequency $\omega(t)$ is determined by a preset open-loop frequency $\hat{\omega}_o$, user-defined proportional-integral (PI) controller gains K_P and K_I and the phase difference $\Delta\varphi(t) = \varphi_\kappa(t) - \hat{\varphi}$ where $\varphi_\kappa(t)$ is the phase lag between the κ-th harmonic of the collocated acceleration and excitation force. The closed-loop control scheme is sketched in Figure 1 and reduces to conventional open-loop testing when the switch is open or when one lets $K_P = K_I = 0$. In this work, our main focus is on PLL testing for tracking primary resonance backbones ($\kappa = 1$); the target phase lag $\hat{\varphi}$ should thus be equal to $\pi/2$ for enforcing phase lag quadrature. However, it is worth noting that the present method can also be extended to identify secondary nonlinear resonances and folded NFRCs [28].

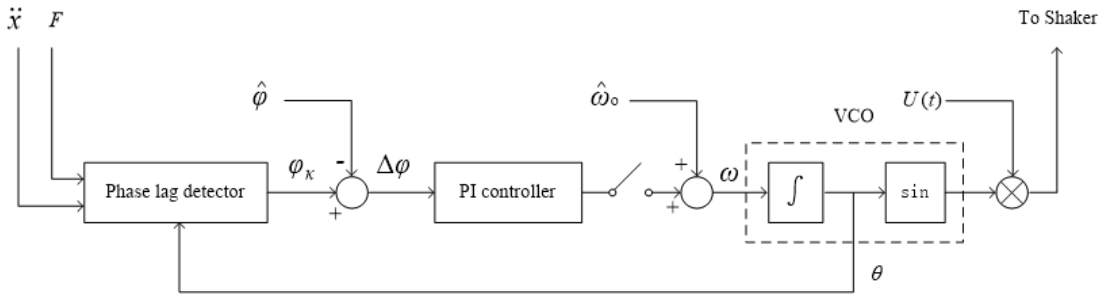

Fig. 1 The PLL control scheme with phase lag estimated using adaptive filtering (see Eqs.(5-10)).

The NNM is identified when the phase lag is converged ($\Delta\varphi(t) \approx 0$) meaning that the phase resonance criterion is fulfilled. At that moment, the system is in steady state and the frequency of excitation is constant, resulting in an equivalence between the open- and closed-loop system dynamics. This implies that after some initial transients, the proportional term of the phase difference $K_P\Delta\varphi(t)$ vanishes and the integral term $K_I \int_0^t \left[\Delta\varphi(\tau)\right] \mathrm{d}\tau$ is equal to the offset between the nonlinear modal frequency ω_{NL} and the open-loop frequency $\hat{\omega}_o$. In other words, the forcing

frequency approximates the modal frequency $\omega(t) \approx \omega_{\mathrm{NL}}$ and the system response corresponds to the nonlinear mode shape $\ddot{\mathbf{x}}(t) \approx \mathbf{\Phi}_{\mathrm{NL}}$.

To extract the instantaneous phase lag required by PLL control, an online Fourier decomposition of the measured acceleration signals is carried out

$$\ddot{x}_n(t) \approx \mathbf{Q}^{\mathrm{T}}(t)\mathbf{z} = z_0 + \sum_{\kappa=1}^{N_H} \left[z_{s\kappa} \sin\left(\kappa\theta(t)\right) + z_{c\kappa} \cos\left(\kappa\theta(t)\right) \right], \tag{5}$$

where the basis vector $\mathbf{Q}(t)$ contains N_H harmonic functions (with instantaneous phase $\theta(t)$ defined by Equation (3)) and the Fourier coefficients $\mathbf{z}$ are updated using adaptive filtering with a least mean-squares algorithm following the discrete adaptation law [29, 30]

$$\mathbf{z}(t_{i+1}) = \mathbf{z}(t_i) + \mu \left[\ddot{x}_n(t_i) - \mathbf{Q}^{\mathrm{T}}(t_i)\mathbf{z}(t_i) \right] \mathbf{Q}(t_i), \tag{6}$$

where μ is the filter gain and t_i is the i-th sample time. The κ-th harmonic at the driving point ($n = d$) is then extracted as

$$\ddot{x}_{d,\kappa}(t) = A_\kappa^a \sin\left(\kappa\theta(t) + \varphi_\kappa^a\right), \tag{7}$$

and the amplitude and phase are determined according to

$$A_\kappa^a = \sqrt{z_{s\kappa}^2 + z_{c\kappa}^2}, \tag{8}$$

and

$$\varphi_\kappa^a = \mathrm{arctan2}(z_{c\kappa}, z_{s\kappa}), \tag{9}$$

respectively. In addition to online phase detection, this adaptive filtering approach can also be utilized as a powerful tool for subsequent offline signal postprocessing tasks, such as time-frequency analysis and the conversion to displacement and velocity responses without relying on low-pass filters.

The forcing phase φ_1^F with respect to the reference voltage phase $\theta(t)$ is evaluated by replacing the acceleration term in (5) and (6) with the measured excitation forcing. This evaluation is used to correct the forcing phase shift in (3) arising from the presence of the shaker in experimental testing. The estimated fundamental harmonic phase lag of the measured acceleration with respect to applied excitation ($\kappa = 1$) is given by

$$\varphi_\kappa \approx \varphi_\kappa^a - \varphi_1^F. \tag{10}$$

Eventually, the backbone can be obtained by gradually increasing the forcing amplitude. In this work, the input voltage magnitude fed to the excitation shaker during backbone tracking follows a ramp-type function and is swept at a constant rate $d|U(t)|/dt = C_r$.

Theoretical studies indicate that nonlinear phase resonance occurs when displacement and forcing are in phase quadrature [27, 31], similar to the behavior of linear systems. However, in practice, mode coupling can cause phase resonance to deviate from $\pi/2$. Therefore, it is recommended to measure a NFRC at a low forcing level to estimate the resonant phase lag $\hat{\varphi}$.

The NNM identification strategy adopted in this paper is as follows:

1. Linear modal analysis and SST are performed to identify the resonant phase lags in the frequency range of interest;
2. At low excitation level, the open-loop frequency $\hat{\omega}_o$ is chosen close to the linear frequency of the target mode and the PI controller is activated so as to reach an initial point on the backbone;
3. The forcing amplitude $\hat{F}$ is gradually increased for the continuation of the backbone curve;
4. The correspondence between the identified backbone curve and the corresponding NFRCs is verified to assess the accuracy of the identification.

III. The F-16 Aircraft and Test Setup

This study was conducted during a Siemens Ground Vibration Testing (GVT) campaign, which took place in September 2023 at the Air Force Campus Saffraanberg in Sint-Truiden, Belgium. As shown in Figure 2, the decommissioned F-16 aircraft was positioned on the ground, and its slightly flattened tires served to provide soft supports to mimic free boundary conditions. Two dummy missiles were mounted on their respective wing tip launchers. Wing-to-payload interfaces are often recognized as a potential source of nonlinearities [2, 25]. A dummy store was attached below the inlet duct, while no payloads were installed under the wing bodies. The equilibrium positions of flight control surfaces, including the flaps connected to the wing trailing edges, the rudder behind the vertical tail and the horizontal tailplane, were not modified by the actuation system during the whole testing procedure.

Two electromagnetic shakers (from The Modal Shop) were positioned beneath the right and left wings near the wing tips, as shown in Figure 2. These shakers can be used to excite the aircraft in the vertical direction (Z-direction as illustrated Figure 3). For dynamical excitation, the shaker fed by a power amplifier was connected by screwing a metallic stinger to the impedance head, which was firmly bounded to the wing structure. The excitation location was positioned near the wing tip, and the maximum forcing achievable was approximately 200 N.

A total of 60 PCB acceleration sensors distributed over the F-16 aircraft were employed for vibrational response measurements. Multi-axial sensors were strategically placed at key positions such as wing tips, resulting in a total number of 108 measured degrees of freedom (DoFs). As depicted in Figure 3, the accelerometer network comprises several subsections, namely the left and right wing bodies, the missiles with the launcher and wing flaps, the aircraft

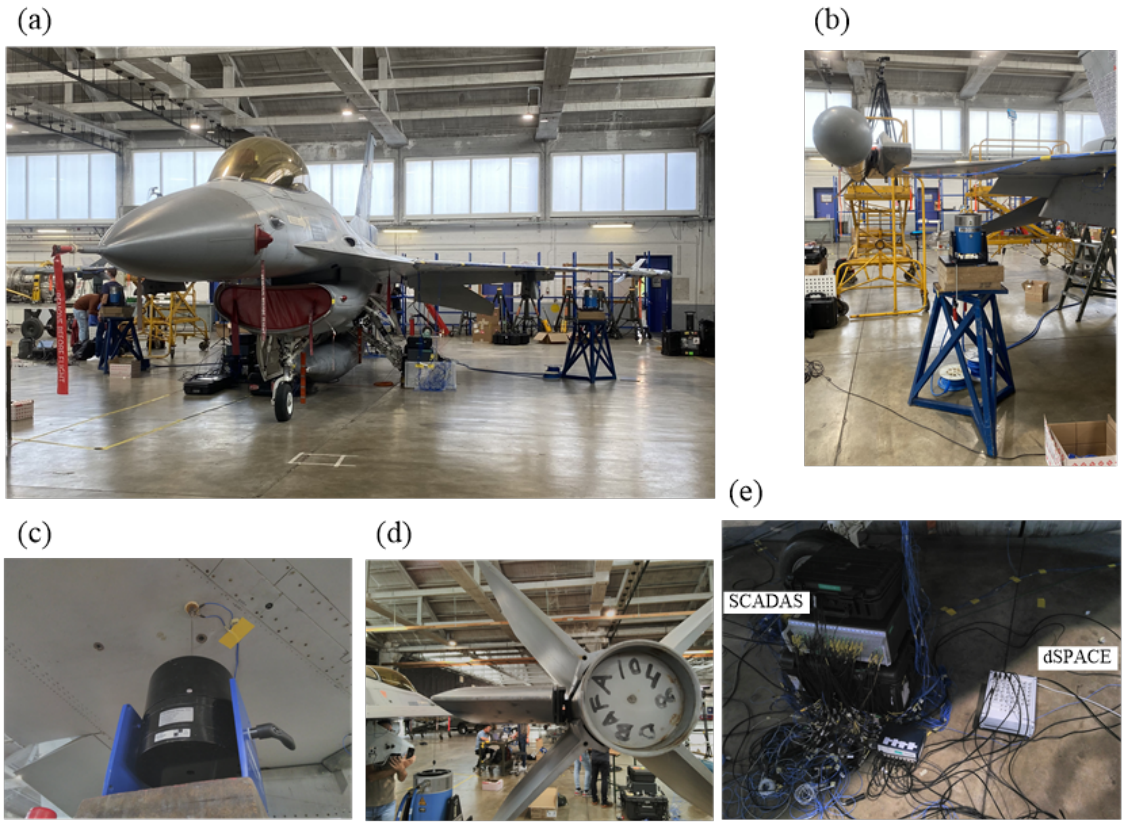

Fig. 2 The F-16 aircraft. (a) The test set-up; (b) the shaker under right wing; (c) the impedance head measuring force and acceleration; (d) right missile; (e) the controller and signal acquisition system.

fuselage, the horizontal tailplanes, the vertical tail and the rudder. The measured response signals were recorded using Simcenter SCADAS data acquisition hardware along with Simcenter Testlab software. The sampling frequency for data acquisition was set to be 800 Hz.

To realize PLL control for NNM identification, we utilized the real-time controller dSPACE MicroLabBox with a sampling frequency set at 10 kHz, and the Matlab/Simulink software to execute the control algorithm. The adaptive filter gain was set to $\mu = 0.001$. For single-point force appropriation, only the electrodynamic shaker underneath the right wing was utilized. The impedance head provided simultaneous measurement of the collocated forcing and acceleration signals. These signals were amplified by a PCB signal conditioner and then transmitted to the dSPACE controller. This setup enabled real-time estimation of the phase lag at the driving point, allowing for the control of the shaker by manipulating the excitation frequency. The feedback loop was formed via an appropriate connection of the controller with the sensor and exciter modules. T-shaped splitters were employed to share acceleration signals between the SCADAS and the MicroLabBox, and two accelerometers at the right wing tip were simultaneously monitored by the controller.

The results of PLL testing were compared against NFRCs obtained via SST in an open-loop excitation setup. While

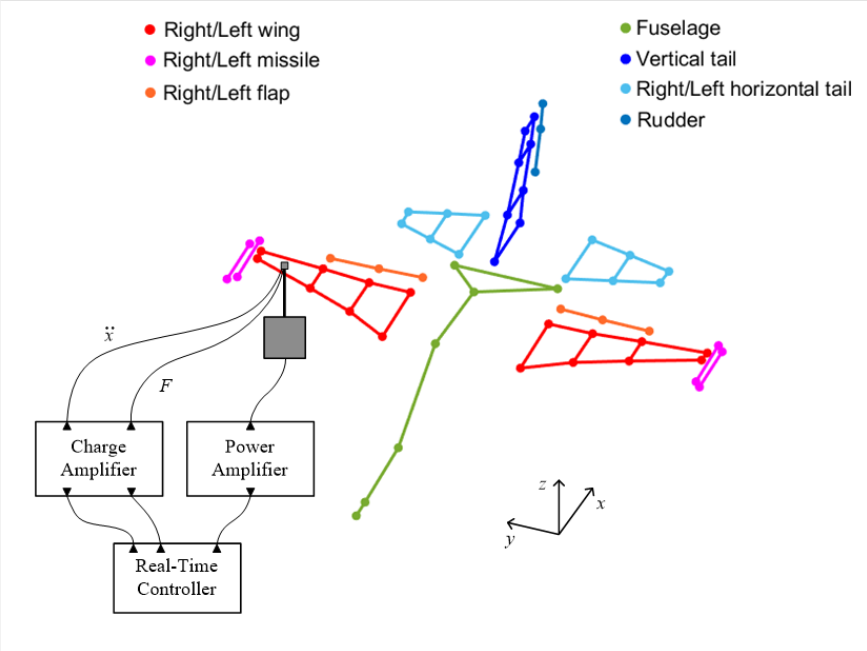

Fig. 3 The sensor network and measurement mesh, with colors indicating individual sections of aircraft. The PLL control setup is also appended.

an additional force controller could potentially enhance force appropriation, it was not employed in this work to avoid potential instabilities. There was no significant variation in forcing amplitude observed during the frequency sweeps.

We note that, besides the identification of the aircraft's primary resonances, we also attempted to identify superharmonic resonances [6]. The evidence for such resonances was brought through a combination of SST and adaptive filtering techniques, by monitoring the amplitudes of higher harmonics .

IV. Experimental Testing and Nonlinear Modal Analysis

A. Linear modal analysis

A prerequisite for nonlinear modal analysis of a complex, multi-mode dynamical system is to have a good knowledge of the underlying linear behavior. Low-level pseudo random excitation with a root-mean-squared (RMS) force amplitude of 11 N was applied by both shakers. The modal parameters were estimated using the PolyMAX method [32]. Four elastic vibration modes involving wing bending and torsion were identified between 5 Hz and 10 Hz. The linear natural frequencies f_{L}, damping ratios ξ_{L} and modal deflection shapes (red lines) are presented in Figure 4, where the gray lines represent the undeformed configuration. The aircraft also features three rigid body modes involving lateral swaying (1.81 Hz), rolling movement (3.36 Hz) and vertical translational motions (3.95 Hz).

The modal synthesis results, carried out based on the stabilization diagram in the frequency band from 1 to 10 Hz, are presented in Figure 5. The gray lines correspond to the Fourier analysis of the experimental data whereas the red

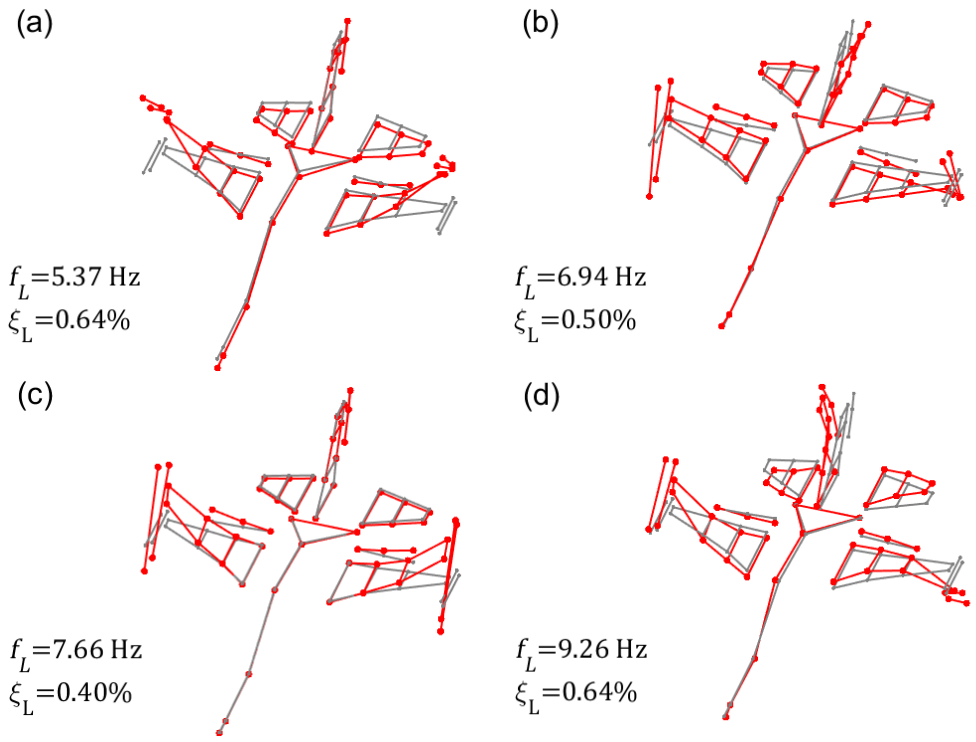

Fig. 4 Linear modal analysis of the (a) first wing bending mode, (b) first, (c) second and (d) fourth wing torsional modes.

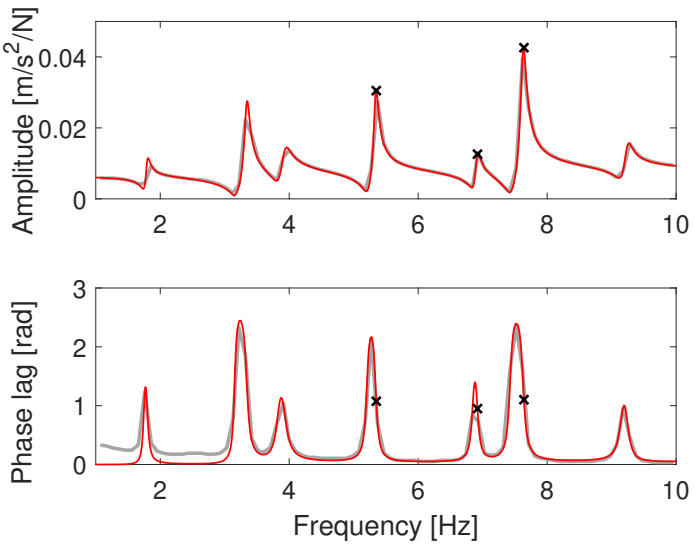

Fig. 5 Amplitude and phase lag of the FRF at the driving point on the right wing.

lines are the modal synthesis results. Surprisingly, the crosses in this figure indicate that the phase lags at amplitude resonance are close to 1 rad for the three considered flexible modes, a significant deviation from the expected theoretical value of $\pi/2$ rad for lighly-damped systems.

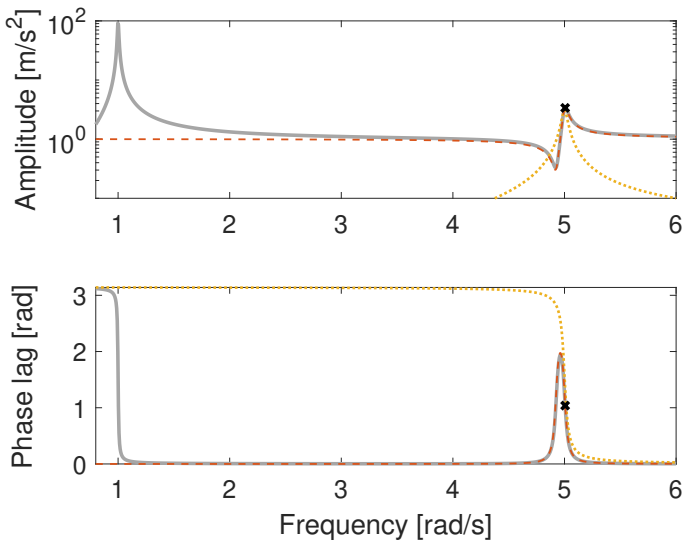

Fig. 6 Amplitude and phase lag of the FRF of a 2DoF linear system. The crosses correspond to the amplitude resonance of the second mode.

The reason for this behavior originates from the fact that the vibration modes are not well-separated in the frequency spectrum. It can be qualitatively explained with a 2DoF linear system. Assuming proportional damping, the driving-point FRF between the force and acceleration has the form [33]

$$\frac{\ddot{x}}{f} = -\frac{\omega^2 a_1^2}{\omega_1^2 - \omega^2 + 2j\xi_1\omega_1\omega} - \frac{\omega^2 a_2^2}{\omega_2^2 - \omega^2 + 2j\xi_2\omega_2\omega}, \tag{11}$$

where ω_i, ξ_i and a_i are the natural frequency, damping ratio and amplitude of mode i, respectively, and j is the unit imaginary number. Near the resonance of the second mode, a single-mode approximation consists in neglecting the first term in Equation (11). A more accurate estimation can be made if one considers the inertia residual of mode 1, i.e., if one neglects terms other than ω^2 in the denominator associated to the first mode (which amounts to neglecting the modal stiffness and damping forces), leading to

$$\frac{\ddot{x}}{f} \approx a_1^2 - \frac{\omega^2 a_2^2}{\omega^2 - \omega_2^2 + 2\mathrm{i}\xi_2\omega_2\omega}, \tag{12}$$

where a_1^2 is the inertia residual of mode 1. Figure 6 present amplitude and phase lag of the FRF of a 2DoF linear system (gray lines), with natural frequencies equal to 1 and 5 rad/s, damping ratios (0.5%, 0.5%) and modal amplitudes equal to 1 and 0.175. The phase evolution of the second mode is strongly influenced by the first mode through its inertia residual. This is evident when comparing the contribution from the second mode alone (yellow lines) with its combination with the inertia residual of the first mode (red lines). An alternative (but essentially similar) way to make this observation is

to note that the antiresonances are generally close to the resonances for which the resonant phase lag deviates from $\pi/2$ rad [34].

Coming back to the F16 test results, it should be noted that the phase evolves monotonously in the vicinity of resonances and that the resonant phase lag value remains the same at different forcing levels. Therefore, appropriate conditions for the application of PLL testing are present, and nonlinear modal analysis can be attempted.

B. Primary resonances of the F-16 aircraft

In this section, we focus on the identification and analysis of the primary resonances of the first three nonlinear elastic vibration modes.

1. Second wing torsion mode

The backbone curve at the driving point for the second wing torsion mode, which exhibits a symmetric wing deflection around 7.7 Hz, was identified using PLL by either sweeping up or down the input voltage fed to the amplifier. The sweep rate was fixed to 0.005 V/s. The NFRCs were obtained through relatively slow SST. The test durations for one run of PLL and SST were around 4 mins and 2 mins, respectively, so the PLL is faster than SST when the objective is to extract nonlinear modal properties.

Figure 7 presents the experimental nonlinear modal analysis results. The backbone curve of the second wing torsion mode was identified by PLL with $K_P = 0.1, K_I = 0.5$. The NFRCs are obtained with SST at $F = 5, 18, 32, 40, 48$ N. The circles and crosses represent phase lags at $\pi/2$ and 1 rad, respectively. This convention applies to subsequent figures as well, unless specified otherwise. The backbone curve is in close agreement with the resonance peaks of the NFRCs confirming that an effective identification took place. Due to nonlinear softening effects, the resonance frequency decreases continuously from the close vicinity of the previously identified linear natural frequency 7.66 Hz, and a discontinuity in the backbone is observed around 7.56 Hz (the vertical dashed line in Figure 7 (a)). On the other hand, the NFRCs are typical of those of frictional systems.

The measured phase lag in Figure 7(b) shows a good convergence toward the target value of 1 rad. As shown in Figure 8, the target phase lag corresponds to the location where amplitude resonance occurs. Different PLL controller gains (K_P and K_I) were considered to demonstrate the reliability and robustness of PLL testing. Figure 9(a) evidences little variability (error consistently below 5%) between the different gain values considered. Figure 9(b) shows that greater controller gains lead to smaller averaged phase lag deviation. Here, the black dashed line refers to the resonant phase lag. The lines below (above) the dashed line correspond to increasing (decreasing) force, with green lines: $K_P = 0.01, K_I = 0.2$ (Downward: $K_I = 0.3$), red lines: $K_P = 0.1, K_I = 0.5$ and blue lines: $K_P = 0.1, K_I = 1.0$. The results discussed in what follows are based on an increasing voltage and $K_P = 0.1, K_I = 1.0$.

The time-frequency analyses, namely adaptive filtering and short-time Fourier transform, in Figure 10 were carried

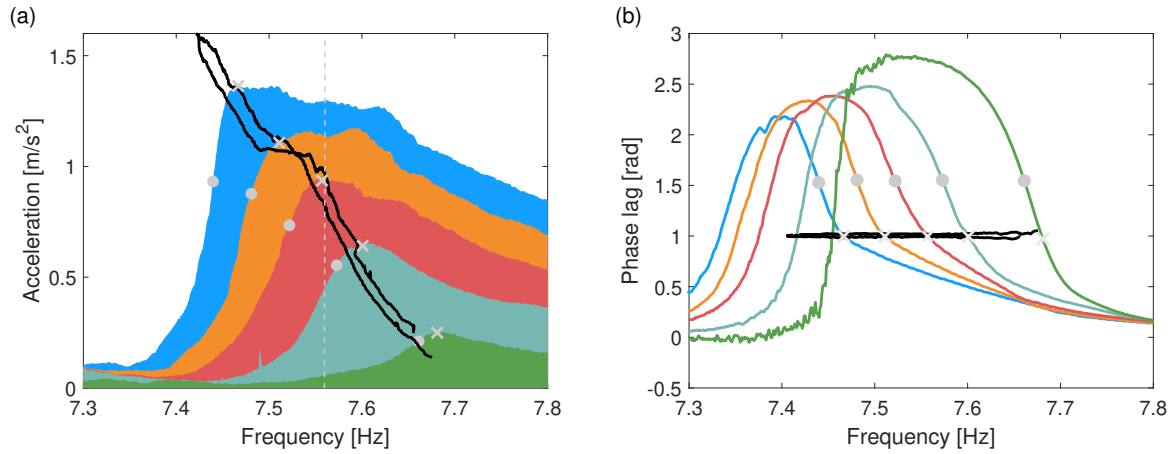

Fig. 7 Backbone curves (black) of the second wing torsion mode identified by PLL and colored NFRCs: (a) amplitude and (b) phase lag.

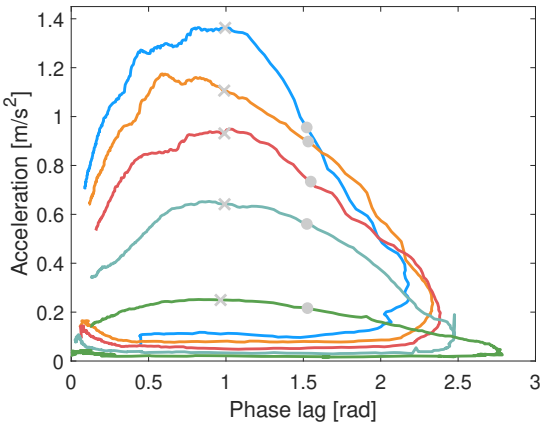

Fig. 8 The relation between response amplitude and phase lag of SST results in Figure 7.

out to evaluate the dominant harmonic components during backbone tracking. The adaptive filter with $N_H = 30$ harmonics in Figure 10(a) can accurately represent the raw data with excellent noise rejection. The fundamental harmonic is seen to dominate the system response. A small jump occurs in the time response near the aforementioned backbone discontinuity. After that, there is an abrupt change in the response envelope's slope, and the presence of a much richer harmonic content is revealed by Figure 10(b). This figure also shows that odd harmonics are greater than the even ones.

The acceleration surface method (ASM) [35], a variant of the restoring force surface method [36], was employed to characterize the aircraft's nonlinearities. Because PLL testing allows for an effective tracking of backbone curves, its combination with the ASM which ideally requires near-resonance condition is thus particularly suitable for nonlinear system identification. To the best of our knowledge, it is the first time that the joint use of the two techniques is proposed.

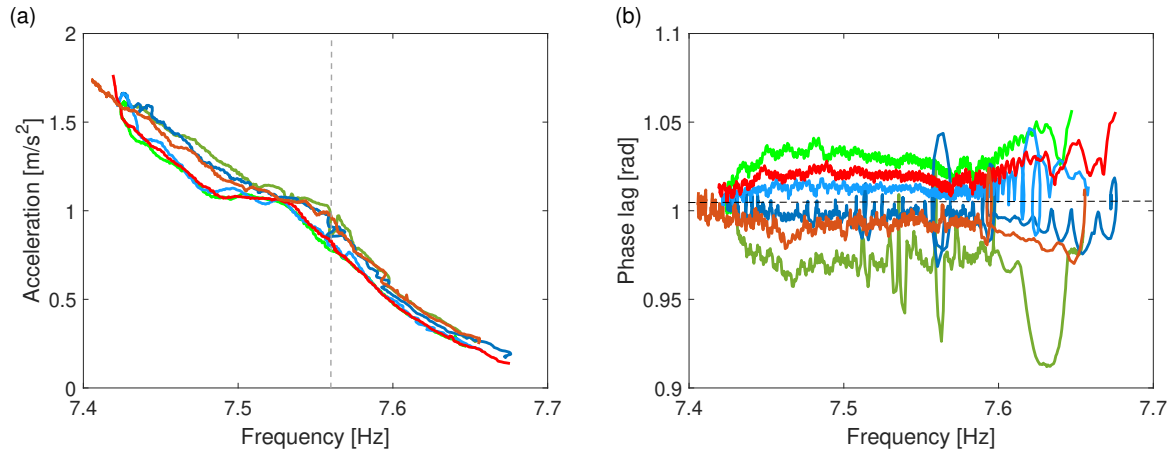

Fig. 9 Backbone curves of the second wing torsion mode identified by PLL using different controller gains: (a) amplitude and (b) phase lag.

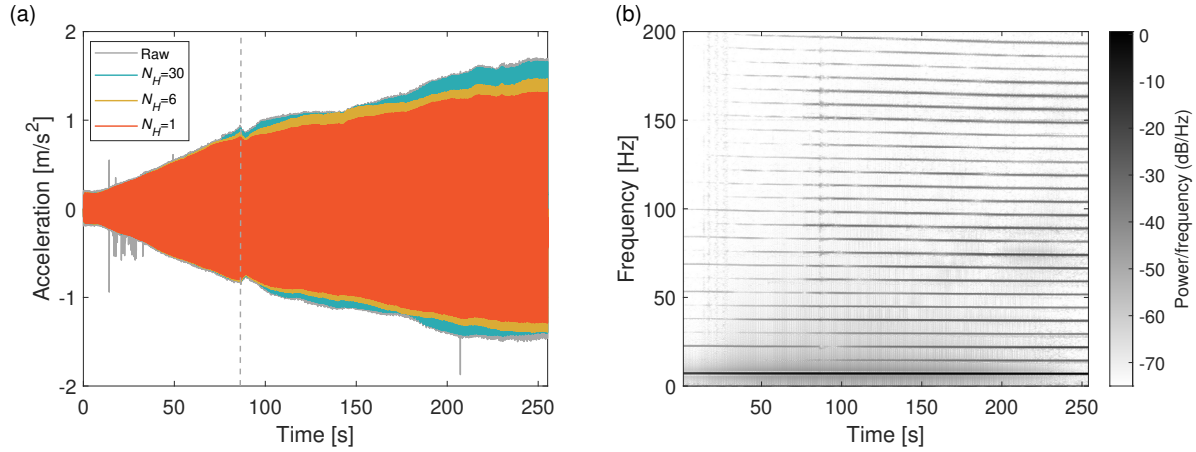

Fig. 10 Time-frequency analysis during backbone tracking ($K_P = 0.1, K_I = 1.0$) with (a) adaptive filtering and (b) short-time Fourier transform.

Figure 11 shows that both elastic and damping nonlinearities appear in the left wingtip launcher. Specifically, Figure 11(a) evidences a trilinear stiffness which leads to an abrupt decrease in the local stiffness as well as the generation of a rich contact-induced harmonic content. This nonsmooth softening nonlinearity is deemed responsible for the discontinuity of the backbone. This is confirmed by checking the time response at the missile side in Figure 12. The damping curve in Figure 11(b) resembles that of Coulomb friction. The decrease in damping force at greater relative velocities could be attributed to joint loosening.

The deviation between the nonlinear mode shape $\mathbf{\Phi}_{\mathrm{NL}}$, given by the operational deflection shape, and the underlying linear mode shape $\mathbf{\Phi}_{\mathrm{L}}$, identified from the stability diagram of the linear modal analysis in Section IV.A, is determined

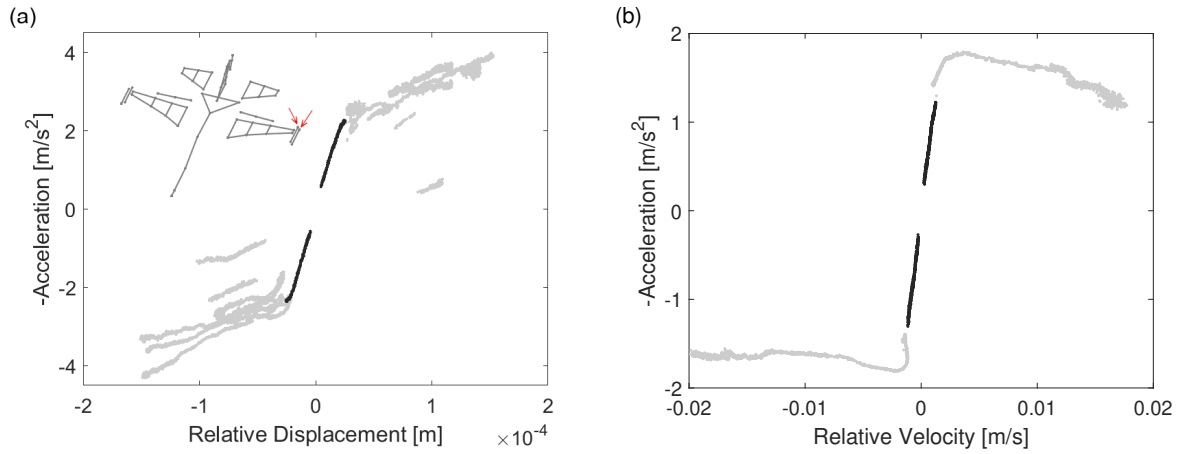

Fig. 11 Acceleration surface method with sensors on either side of the left wingtip launcher: (a) stiffness and (b) damping curves. Dark and light gray points indicate pre- and post-discontinuity zones.

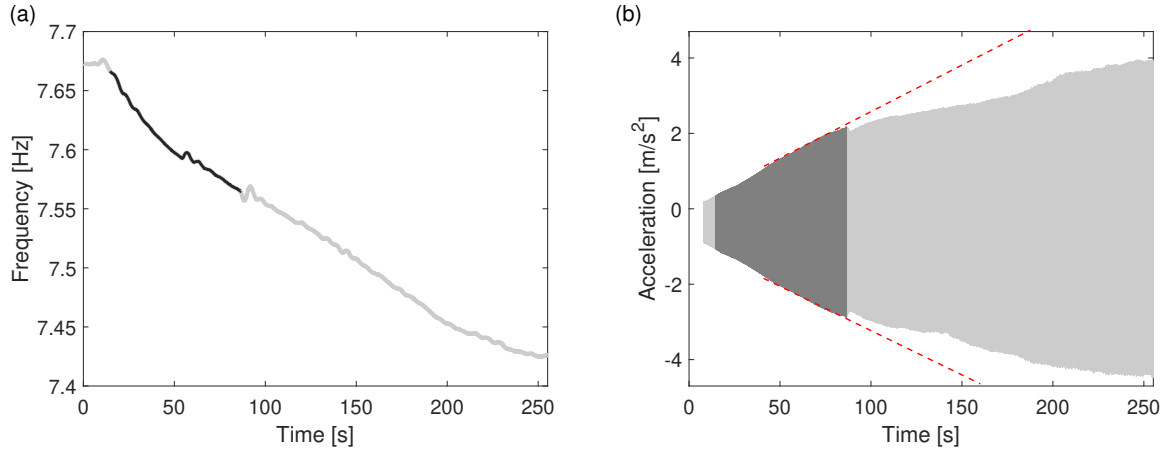

Fig. 12 (a) Time-frequency relation during backbone tracking and (b) time responses at the missile side in Figure 11. The red dashed line is an extrapolation of the pre-discontinuity zone.

using the modal assurance criterion (MAC)

$$\mathrm{MAC} = \frac{\|\boldsymbol{\Phi}_{\mathrm{L}}^{\mathrm{T}}\boldsymbol{\Phi}_{\mathrm{NL}}\|^2}{\|\boldsymbol{\Phi}_{\mathrm{L}}\|^2\|\boldsymbol{\Phi}_{\mathrm{NL}}\|^2}. \tag{13}$$

The MAC was also calculated between the fundamental harmonic component of the nonlinear mode shape $\boldsymbol{\Phi}_{\mathrm{NL},1}$ and $\boldsymbol{\Phi}_{\mathrm{L}}$. Figure 13 displays both MAC values calculated all along the backbone curve. The MAC for the fundamental harmonic component is close to unity indicating that the operational deflection shape identified by PLL control is primarily dominated by a single nonlinear mode and a good nonlinear mode identification has been achieved. Only very minor contributions from other modes influence vibration amplitude, while their effects are primarily reflected in phase lag deviations. On the other hand, the MAC accounting for the higher harmonics departs from unity underlining the

influence of these harmonics. Specifically, the MAC significantly decreases after the discontinuity observed during backbone tracking.

Another relevant indicator is the power-based mode indicator function (PBMIF) defined as the ratio of the active power over apparent power [17]. The PBMIF exhibited little fluctuations during each PLL test and the averaged value was around 0.85, which indicates a good-quality NNM isolation (e.g., the lowest PBMIF in [17] is 0.65 for a beam with a localized nonlinear connection).

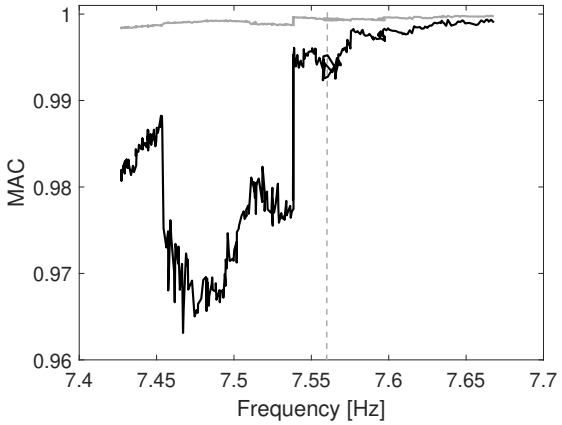

Fig. 13 MAC values: $\mathbf{\Phi}_{\mathrm{NL}}$ (black) and $\mathbf{\Phi}_{\mathrm{NL},1}$ (gray).

Following [20], a nonlinear damping ratio can be defined to characterize the energy dissipation in a nonlinear mechanical system

$$\xi_{\mathrm{NL}} = \frac{P_1}{\omega_{\mathrm{NL}}^3 a^2}. \tag{14}$$

$P_1 = 0.5 F_1 V_1 \cos\bar{\varphi}$ is the fundamental harmonic component of the active power provided by the excitation, where F_1, V_1 and $\bar{\varphi}$ represents the force magnitude, velocity amplitude and phase lag, respectively. Here, ω_{NL} is the nonlinear modal frequency and a is the modal amplitude, which is the amplification factor from the mass-normalized fundamental harmonic mode shape to the unscaled one, i.e. the fundamental harmonic of $\mathbf{x}$. The minor displacement contribution from off-targeted modes and effects of higher harmonics have been neglected. In this work, instead of estimating mass-normalized mode shapes, the proportionality relation is exploited and the nonlinear damping ratio at a low forcing level is assumed to be equal to the linear damping ratio. Figure 14 displays the resulting damping ratio; it increases by a factor of around two with increased vibration amplitudes and decreased frequencies, typical of frictional systems. The damping ratio also decreases slightly at high response levels, consistent with the damping force identified in Figure 11(b).

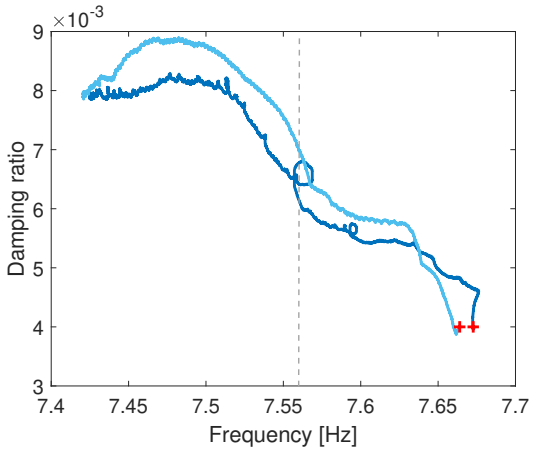

Fig. 14 Nonlinear damping ratios estimated from the identified backbone. The crosses represent the linear case.

2. First wing torsion mode

Figure 15 presents the nonlinear modal testing results for the asymmetric torsion mode near 6.9 Hz. The SST responses at $F = 5, 15, 30$ N indicate that the dynamics for this mode are somewhat more complex. For this mode, only a sweep down of the voltage was considered during backbone tracking (PLL using $K_P = 0.01, K_I = 0.05$), because starting from a low voltage level tended to activate the first wing bending mode. In addition to the softening due to friction, the backbone curve undergoes a pronounced change in curvature. The fundamental phase lag at the driving point remains almost constant (phase deviation less than 0.1 rad) during the test.

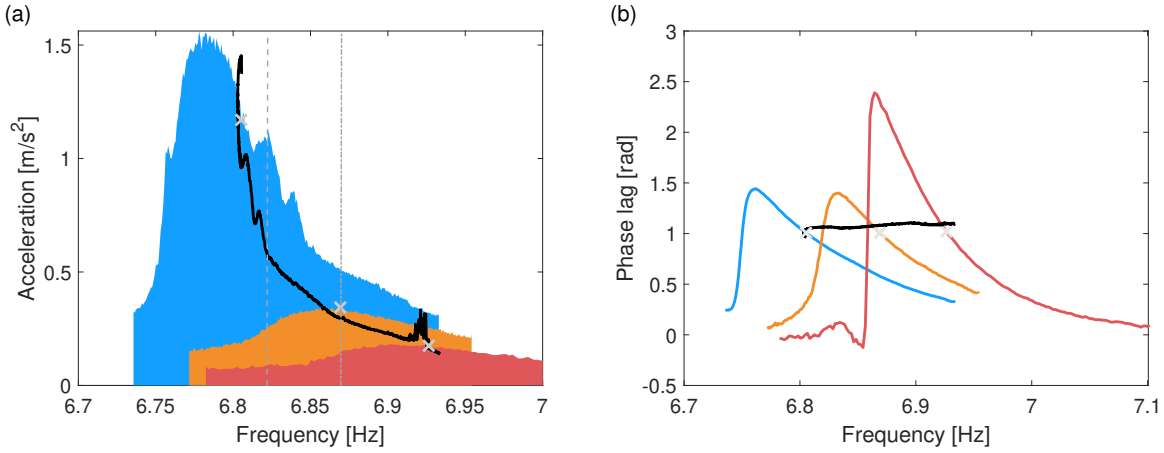

Fig. 15 Backbone curve (black) of the first wing torsion mode and colored NFRCs: (a) amplitude at the right wing tip and (b) fundamental phase lag at the driving point.

Time-frequency analysis is depicted in Figure 16. Compared to the second wing torsion mode, the adaptive filters needed more harmonics ($N_H = 300$) to accurately capture the dynamical behavior. Three distinct vibration regimes can be identified from right to left: friction-dominant (Regime I), harmonic growth (Regime II), and strong contact

interactions (Regime III). In Regime I, at low force magnitudes, the response is primarily governed by the fundamental harmonic, and the system exhibits friction-induced softening. In Regime II, a slight asymmetry emerges in the time response, accompanied by the growth of higher harmonics. Regime III is characterized by a rich harmonic spectrum and pronounced nonsmooth behavior due to strong contact interactions. The time-dependent spectrum, obtained via short-time Fourier transform, further highlights the presence of contacts, with numerous harmonics visible before 80 seconds.

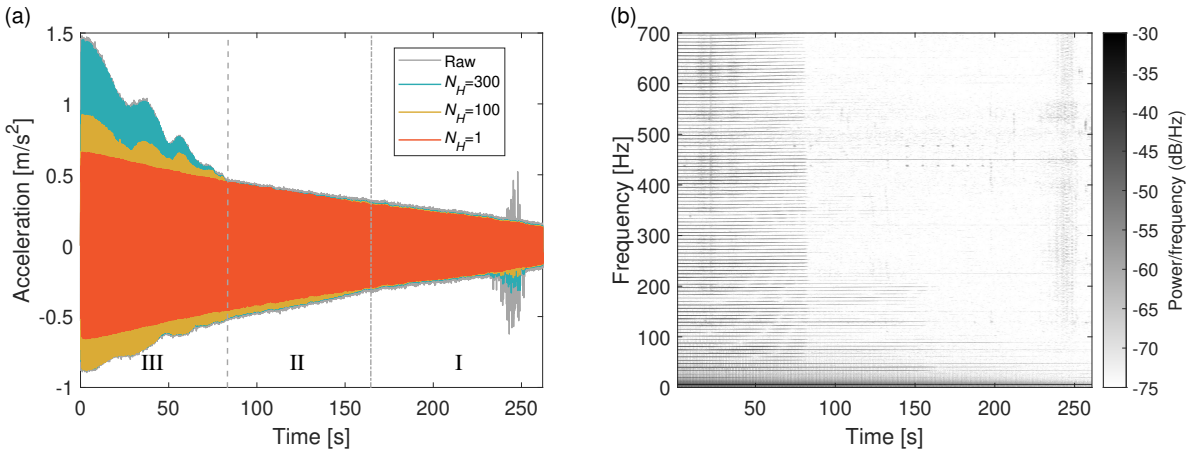

Fig. 16 Time-frequency analysis during backbone tracking (corresponding to the black curve in Figure 15) with (a) adaptive filtering and (b) short-time Fourier transform.

The time responses of the wing body and the flap in the chord direction were examined to have a better understanding of the modal deflection shapes and the underlying nonlinear mechanisms. At high forcing level, Figure 17 evidences that, along the right wing chord line, higher oscillations occur at the back of the wing and at the flap compared to those at the front of the wing. One can also recognize the 3 aforementioned regimes in these time series. The corresponding motions in phase space are represented in Figure 18. Large deviations from an ellipse indicate strong nonlinearities. The wing-to-flap connection thus seems to be the source of contacts for the first wing torsion mode. The mode shapes of the right wing are depicted in Figure 19 and display important deflections next to wing-to-flap connection.

3. First wing bending mode

The backbone curve and NFRCs of the first wing bending mode in Figure 20 exhibit an oscillatory envelope at higher forcing levels, which is mainly induced by the contacts existing in the system. Here, the backbone curve was identified by PLL using $K_P = 0.01, K_I = 0.2$ and The vertical dashed line indicates the location of the onset of contacts. The colored NFRCs are obtained with SST at $F = 4, 10, 20$ N. This mode also features friction-induced softening and the frequency shift is around 2%.

The time-frequency analysis in Figure 21(b) clearly reveals when contacts occur. Around 100 harmonics are

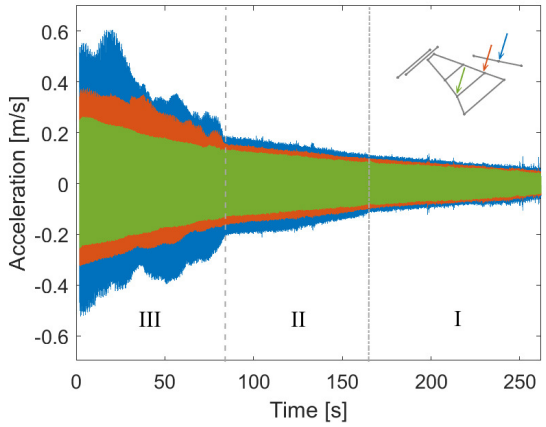

Fig. 17 Time responses along the right wing chord line.

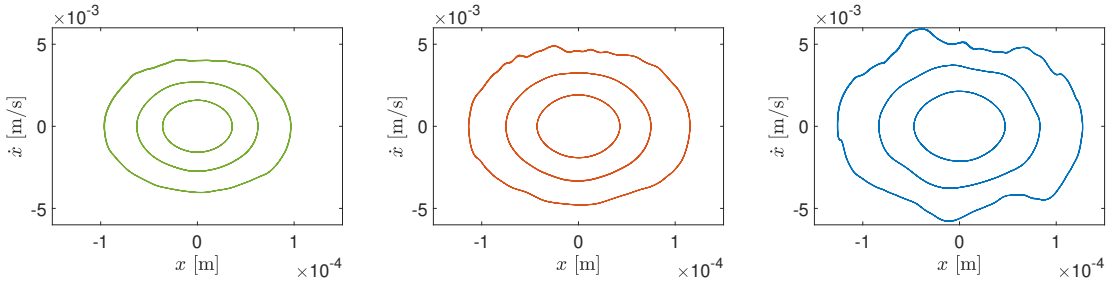

Fig. 18 Motions of three measurement locations in Figure 17 projected in the phase space around 200s, 100s and 20s.

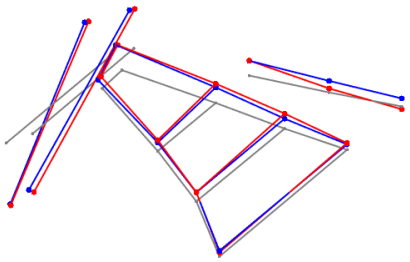

Fig. 19 The aircraft ring wing defection at 250s (blue) and 50s (red), with undeformed mesh as gray.

needed in Figure 21(a) to capture accurately the dynamical behavior. The time responses measured at one wing-to-flap connection interface in Figure 22 also features clear evidence of impacts. The PBMIF is around 0.86, which supports a good nonlinear mode isolation. Due to friction, the damping ratio in Figure 23 increases with increased vibration levels and decreased modal frequencies.

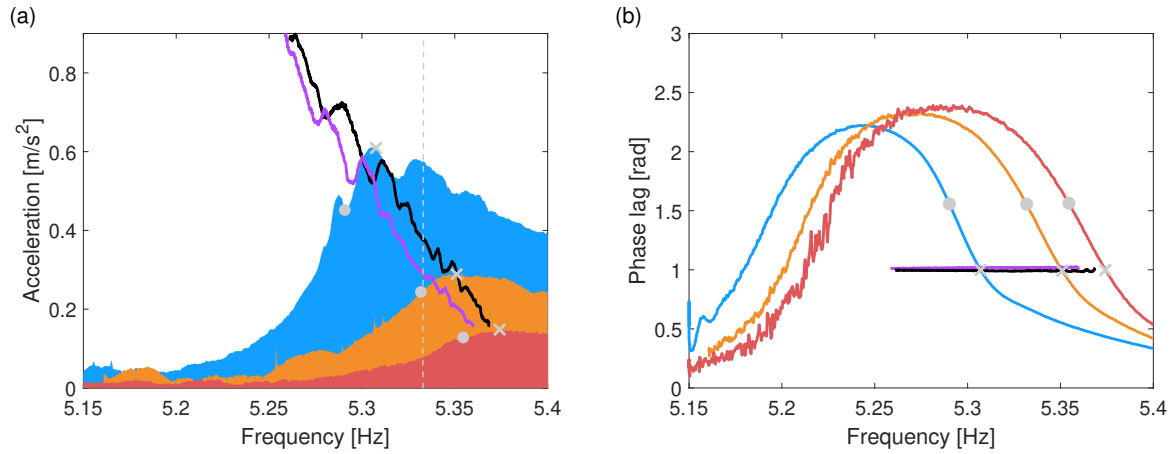

Fig. 20 Backbone curves (black: increasing forcing level, and purple: decreasing forcing level) of the first wing bending mode and colored NFRCs: (a) amplitude and (b) phase lag.

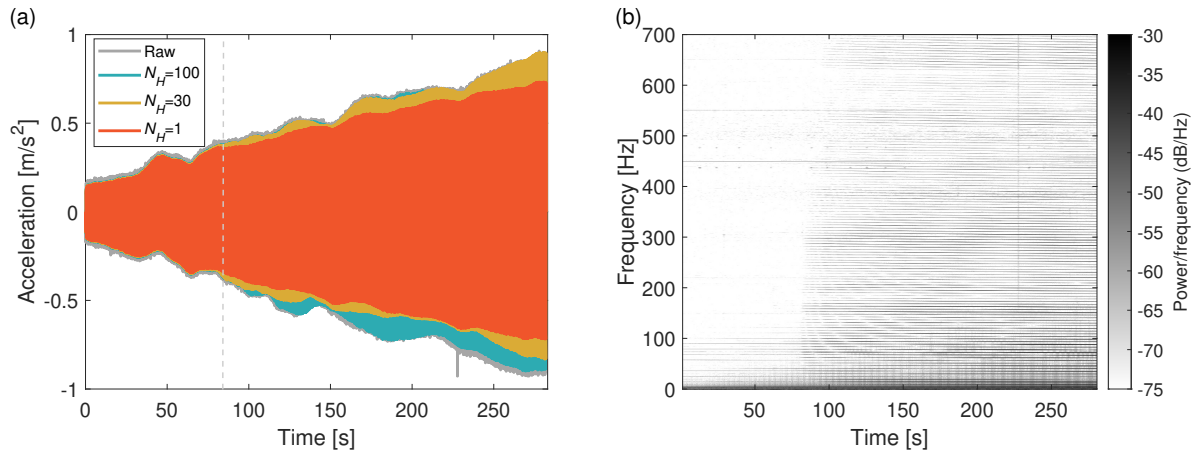

Fig. 21 Time-frequency analysis during backbone tracking for increasing forcing with (a) adaptive filtering and (b) short-time Fourier transform.

C. Superharmonic resonances of the F-16 aircraft

1. Second wing torsion mode

A unique feature of nonlinear systems is the existence of secondary resonances, namely superharmonic and subharmonic resonances [6]. A 3:1 superharmonic resonance of the second wing torsion mode was detected around one third of its linear modal frequency, i.e., 2.58 Hz, using sine sweeps (F = 48 N) and adaptive filtering. The superharmonic resonance peak can be seen in Figure 24(a), which represents the frequency response of the third harmonic of the response. This third harmonic is admittedly very small, explaining its noisy behavior, but, at the same time, this demonstrates the effectiveness of adaptive filters. Figure 24(b) reveals that the phase lag between the third harmonic of the response and the forcing is near $\pi/2$ rad (the crosses represent phase resonance), in agreement with the theoretical

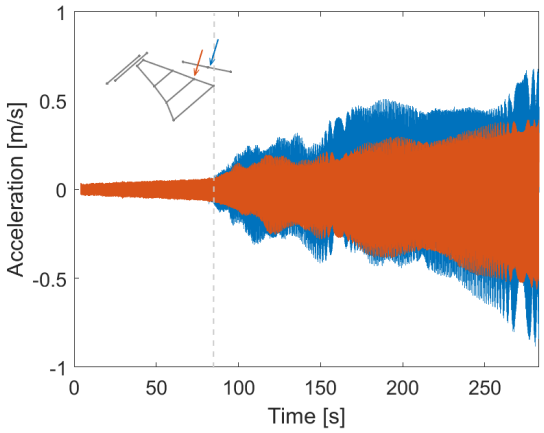

Fig. 22 Time responses measured at a wing-to-flap connection interface.

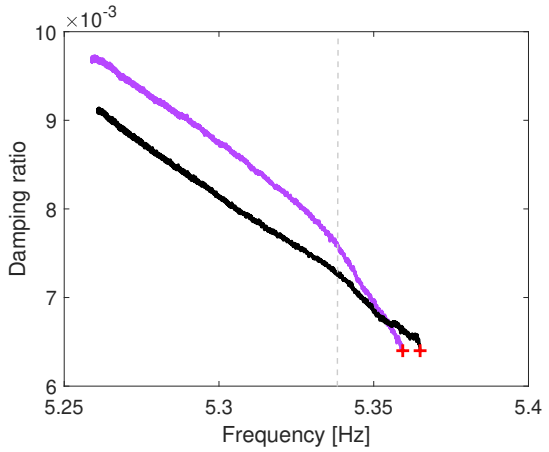

Fig. 23 Nonlinear damping ratio of the first wing bending mode. Black: increasing forcing level, and purple: decreasing forcing level.

value [37]. The deflection shape of the third harmonic at the superharmonic resonance in Figure 24(c) is in close correspondence with the second wing torsion mode shape in Figure 4(c), further confirming that an interaction with this mode takes place. More responsive superharmonic resonances could have probably been obtained with higher forcing levels. Unfortunately, this was not possible considering the shakers used during the tests.

2. Third wing torsion mode

A 3:1 superharmonic resonance of the third wing torsion mode was also identified at $F = 40$ N in Figure 25(a). The deflection shape of the third harmonic in Figure 25(c) indeed resembles the mode shape in Figure 4(d). Figure 25(b) highlights that the resonant phase lag is $3\pi/2$ rad (the crosses represent phase resonance). A possible reason for the phase shift by π is that the superharmonic resonance is close to the rigid-body mode featuring rolling motion, as discussed in [38]. This is confirmed by checking the fundamental harmonic response in Figure 25(d).

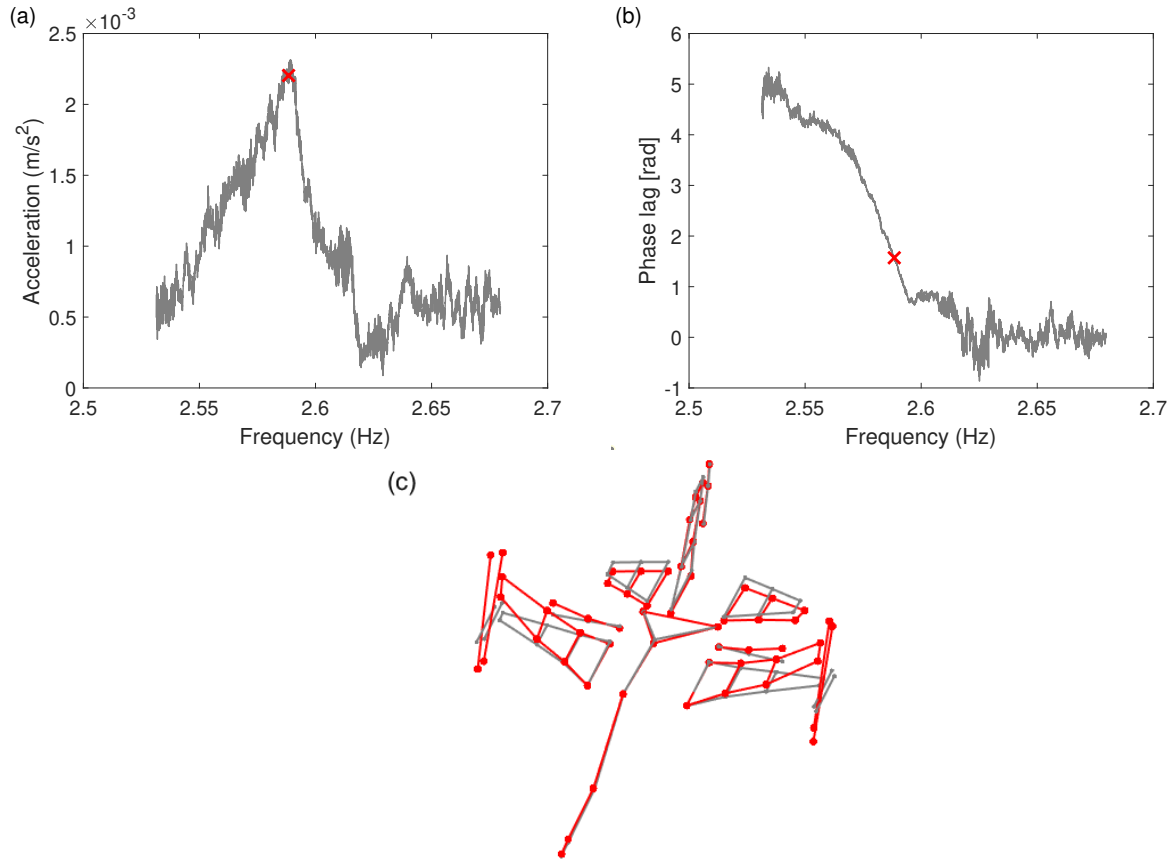

Fig. 24 3:1 superharmonic resonance of the second wing torsion mode: (a) third harmonic FRC, (b) phase lag and (c) deflection shape of the third harmonic.

V. Conclusions

In this study, our focus was on the experimental identification of wing bending and torsion modes in a full-scale F-16 aircraft. To achieve this, we employed Phase-Locked Loop (PLL) testing, which utilizes adaptive filtering for real-time phase lag calculation and a PI controller to maintain the response at the desired resonant phase lag. Given the limited availability of the F-16, all tests were completed in under six hours, highlighting the efficiency and robustness of the PLL testing method.

The backbone curves were successfully identified for the aircraft's first wing bending mode as well as its first and second torsion modes. These curves closely matched the maxima of the nonlinear frequency responses obtained from sine sweep testing. An interesting finding of this study is that the resonant phase lags deviated from $\pi/2$, likely due to the imperfect separation of the aircraft modes. This contrasts with the typical behavior observed in the literature on isolated nonlinear mode identification [14, 17, 18]. Two 3:1 superharmonic resonances, corresponding to the second and third torsion modes, were also measured during the sine sweeps. These resonances occurred at very low acceleration levels, highlighting the effectiveness of the adaptive filtering process proposed in [30].

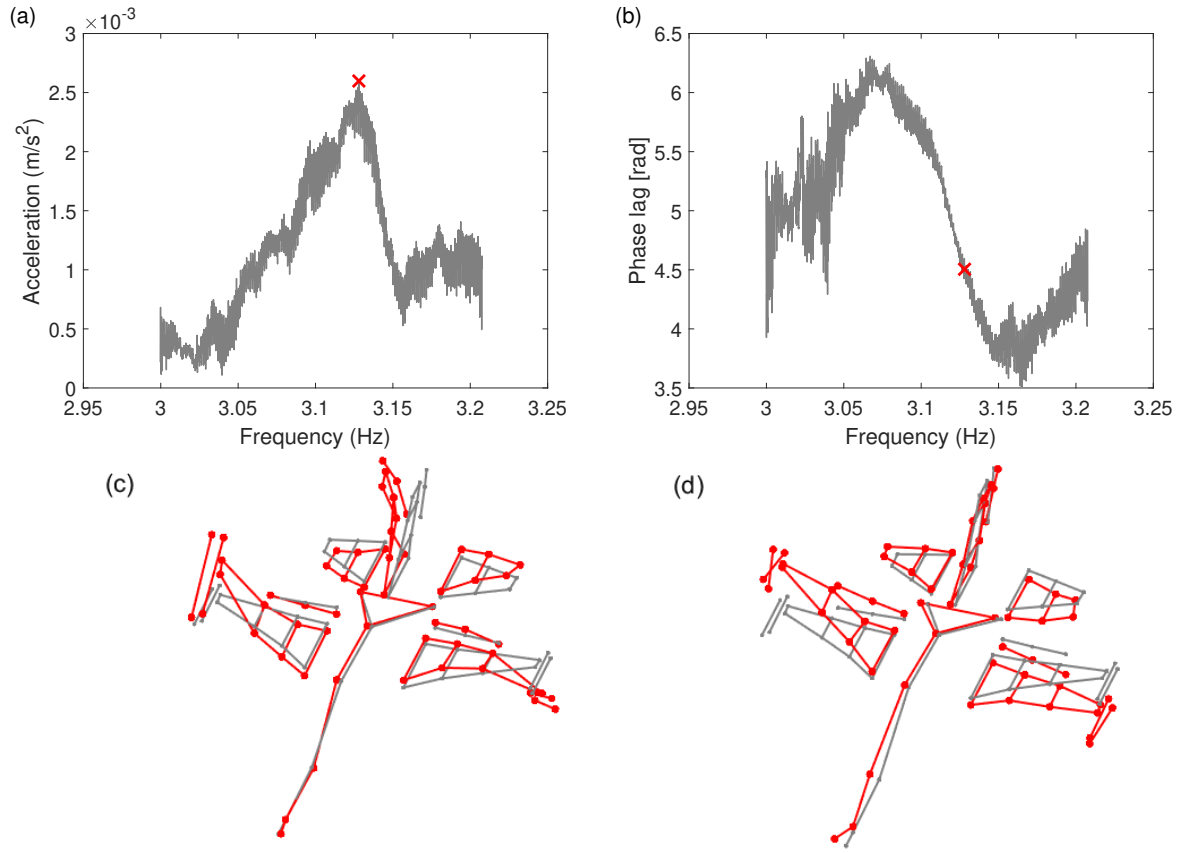

Fig. 25 3:1 superharmonic resonance of the third wing torsion mode: (a) third harmonic FRC, (b) phase lag, deflection shapes of (c) third and (d) fundamental harmonics.

Finally, two sources of nonlinearity were identified in the aircraft: one in the wingtip launcher and another at the wing-to-flap connection. The nonlinearity in the wingtip launcher was characterized using a unique combination of the ASM method [35] and PLL testing, revealing a trilinear softening stiffness and Coulomb damping.

Acknowledgments

Tong Zhou gratefully acknowledges the financial support provided by the postdoctoral fellowship at University of Liege (IPD-STEMA 2021, R.DIVE.0981-J-F-L). Ghislain Raze is a Postdoctoral Researcher of the Fonds de la Recherche Scientifique - FNRS which is gratefully acknowledged.

References

[1] Göge, D., Böswald, M., Füllekrug, U., and Lubrina, P., "Ground Vibration Testing of Large Aircraft–State-of-the-Art and Future Perspectives," *25th International Modal Analysis Conference*, 2007.

[2] Kerschen, G., Peeters, M., Golinval, J.-C., and Stéphan, C., "Nonlinear Modal Analysis of a Full-Scale Aircraft," *Journal of*

Aircraft, Vol. 50, No. 5, 2013, pp. 1409–1419. https://doi.org/https://doi.org/10.2514/1.C031918.

[3] Zou, Q., Huang, R., Mu, X., Hu, H., Fan, Z., and Liu, H., "Body-freedom Flutter Analysis and Flight Test for a Flying-wing Aircraft Testbed," *Mechanical Systems and Signal Processing*, Vol. 221, 2024, p. 111717. https://doi.org/https://doi.org/10.1016/j.ymssp.2024.111717.

[4] Akers, J., Winkel, J., Chin, A., Parks., R., Chandler, D., Stasiunas, E., and Allen, M., "Operational Modal Analysis of the Artemis I Dynamic Rollout Test and Wet Dress Rehearsal," *International Modal Analysis Conference (IMAC) XLII*, 2024, pp. 91–112. https://doi.org/https://doi.org/10.1007/978-3-031-68188-2_10.

[5] Noël, J.-P., and Kerschen, G., "Nonlinear System Identification in Structural Dynamics: 10 More Years of Progress," *Mechanical Systems and Signal Processing*, Vol. 83, 2017, pp. 2–35. https://doi.org/https://doi.org/10.1016/j.ymssp.2016.07.020.

[6] Nayfeh, A., and Mook, D., *Nonlinear oscillations*, John Wiley & Sons, 2008. https://doi.org/DOI:10.1002/9783527617586.

[7] Rosenberg, R., "Normal Modes of Nonlinear Dual-Mode Systems," *Journal of Applied Mechanics*, Vol. 27, No. 2, 1960, pp. 263–268. https://doi.org/https://doi.org/10.1115/1.3643948.

[8] Kerschen, G., Peeters, M., Golinval, J.-C., and Vakakis, A., "Nonlinear Normal Modes, Part I: A Useful Framework for the Structural Dynamicist," *Mechanical systems and signal processing*, Vol. 23, No. 1, 2009, pp. 170–194. https://doi.org/https://doi.org/10.1016/j.ymssp.2008.04.002.

[9] Shaw, S., and Pierre, C., "Non-linear Normal Modes and Invariant Manifolds," *Journal of sound and Vibration*, Vol. 150, No. 1, 1991, pp. 170–173. https://doi.org/https://doi.org/10.1016/0022-460X(91)90412-D.

[10] Haller, G., and Ponsioen, S., "Nonlinear Normal Modes and Spectral Submanifolds: Existence, Uniqueness and Use in Model Rreduction," *Nonlinear Dynamics*, Vol. 86, No. 3, 2016, pp. 1493–1534. https://doi.org/10.1007/s11071-016-2974-z.

[11] Axås, J., Cenedese, M., and Haller, G., "Fast Data-Driven Model Reduction for Nonlinear Dynamical Systems," *Nonlinear Dynamics*, Vol. 111, No. 9, 2023, pp. 7941–7957. https://doi.org/https://doi.org/10.1007/s11071-022-08014-0.

[12] Renson, L., Hill, T. L., Ehrhardt, D. A., Barton, D. A. W., and Neild, S. A., "Force Appropriation of Nonlinear Structures," *Proceedings of the Royal Society A: Mathematical, Physical and Engineering Sciences*, Vol. 474, 2018. https://doi.org/https://doi.org/10.1098/rspa.2017.0880.

[13] Peeters, M., Kerschen, G., and Golinval, J.-C., "Dynamic Testing of Nonlinear Vibrating Structures using Nonlinear Normal Modes," *Journal of Sound and Vibration*, Vol. 330, No. 3, 2011, pp. 486–509. https://doi.org/https://doi.org/10.1016/j.jsv.2010.08.028.

[14] Peeters, M., Kerschen, G., and Golinval, J.-C., "Modal Testing of Nonlinear Vibrating Structures Based on Nonlinear Normal Modes: Experimental Demonstration," *Mechanical Systems and Signal Processing*, Vol. 25, No. 4, 2011, pp. 1227–1247. https://doi.org/https://doi.org/10.1016/j.ymssp.2010.11.006.

[15] Breunung, T., and Haller, G., "Explicit Backbone Curves from Spectral Submanifolds of Forced-damped Nonlinear Mechanical Systems," *Proceedings of the Royal Society A: Mathematical, Physical and Engineering Sciences*, Vol. 474, No. 2213, 2018, p. 20180083. https://doi.org/10.1098/rspa.2018.0083.

[16] Debeurre, M., Benacchio, S., Grolet, A., Grenat, C., Giraud-Audine, C., and Thomas, O., "Phase Resonance Testing of Highly Flexible Structures: Measurement of Conservative Nonlinear Modes and Nonlinear Damping Identification," *Mechanical Systems and Signal Processing*, Vol. 215, No. February, 2024, p. 111423. https://doi.org/10.1016/j.ymssp.2024.111423.

[17] Peter, S., and Leine, R., "Excitation Power Quantities in Phase Resonance Testing of Nonlinear Systems with Phase-Locked-Loop Excitation," *Mechanical Systems and Signal Processing*, Vol. 96, 2017, pp. 139–158. https://doi.org/https://doi.org/10.1016/j.ymssp.2017.04.011.

[18] Denis, V., Jossic, M., Giraud-Audine, C., Chomette, B., Renault, A., and Thomas, O., "Identification of Nonlinear Modes Using Phase-Locked-Loop Experimental Continuation and Normal Form," *Mechanical Systems and Signal Processing*, Vol. 106, 2018, pp. 430–452. https://doi.org/https://doi.org/10.1016/j.ymssp.2018.01.014.

[19] Abeloos, G., Müller, F., Ferhatoglu, E., Scheel, M., Collette, C., Kerschen, G., Brake, M., Tiso, P., Renson, L., and Krack, M., "A Consistency Analysis of Phase-Locked-Loop Testing and Control-Based Continuation for a Geometrically Nonlinear Frictional System," *Mechanical Systems and Signal Processing*, Vol. 170, 2022, p. 108820. https://doi.org/https://doi.org/10.1016/j.ymssp.2022.108820.

[20] Scheel, M., Peter, S., Leine, R., and Krack, M., "A Phase Resonance Approach for Modal Testing of Structures with Nonlinear Dissipation," *Journal of Sound and Vibration*, Vol. 435, 2018, pp. 56–73. https://doi.org/https://doi.org/10.1016/j.jsv.2018.07.010.

[21] Bhattu, A., Hermann, S., Jamia, N., Müller, F., Scheel, M., Schwingshackl, C., Özgüven, N., and Krack, M., "Experimental Analysis of the TRC Benchmark System," *Journal of Structural Dynamics*, Vol. Special issue on Tribomechadynamics, 2024. https://doi.org/DOI:10.25518/2684-6500.206.

[22] Givois, A., Tan, J.-J., Touzé, C., and Thomas, O., "Backbone Curves of Coupled Cubic Oscillators in One-to-One Internal Resonance: Bifurcation Scenario, Measurements and Parameter Identification," *Meccanica*, Vol. 55, No. 3, 2020, pp. 481–503. https://doi.org/https://doi.org/10.1007/s11012-020-01132-2.

[23] Woiwode, L., and Krack, M., "Experimentally Uncovering Isolas via Backbone Tracking." *Journal of Structural Dynamics*, Vol. 2, 2024, pp. 122–143. https://doi.org/DOI:10.25518/2684-6500.180.

[24] Schwarz, S., Kohlmann, L., Hartung, A., Gross, J., Scheel, M., and Krack, M., "Validation of a Turbine Blade Component Test with Frictional Contacts by Phase-Locked-Loop and Force-Controlled Measurements," *Journal of Engineering for Gas Turbines and Power*, Vol. 142, No. 5, 2020, p. 051006. https://doi.org/https://doi.org/10.1115/1.4044772.

[25] Noël, J.-P., Renson, L., Kerschen, G., Peeters, B., Manzato, S., and Debille, J., "Nonlinear Dynamic Analysis of an F-16 Aircraft using GVT Data," *International Forum on Aeroelasticity and Structural Dynamics, IFASD 2013*, Royal Aeronautical Society, 2014, pp. 990–1002.

[26] Peeters, M., Viguié, R., Sérandour, G., Kerschen, G., and Golinval, J.-C., "Nonlinear Normal Modes, Part II: Toward a Practical Computation Using Numerical Continuation Techniques," *Mechanical systems and signal processing*, Vol. 23, No. 1, 2009, pp. 195–216. https://doi.org/https://doi.org/10.1016/j.ymssp.2008.04.003.

[27] Cenedese, M., and Haller, G., "How do conservative backbone curves perturb into forced responses? A Melnikov function analysis," *Proceedings of the Royal Society A: Mathematical, Physical and Engineering Sciences*, Vol. 476, No. 2234, 2020, p. 20190494. https://doi.org/10.1098/rspa.2019.0494.

[28] Zhou, T., and Kerschen, G., "Identification of Secondary Resonances of Nonlinear Systems using Phase-Locked Loop Testing," *Journal of Sound and Vibration*, 2024, p. 118549. https://doi.org/https://doi.org/10.1016/j.jsv.2024.118549.

[29] Haykin, S., *Adaptive Filter Theory*, Prentice Hall, 1996.

[30] Abeloos, G., Renson, L., Collette, C., and Kerschen, G., "Stepped and Swept Control-Based Continuation Using Adaptive Filtering," *Nonlinear Dynamics*, Vol. 104, No. 4, 2021, pp. 3793–3808. https://doi.org/https://doi.org/10.1007/s11071-021-06506-z.

[31] Volvert, M., and Kerschen, G., "Resonant Phase Lags of a Duffing Oscillator," *International Journal of Non-Linear Mechanics*, Vol. 146, No. July, 2022, p. 104150. https://doi.org/10.1016/j.ijnonlinmec.2022.104150.

[32] Peeters, B., Van der Auweraer, H., Guillaume, P., and Leuridan, J., "The PolyMAX Frequency-Domain Method: a New Standard for Modal Parameter Estimation ?" *Shock and Vibration*, Vol. 11, No. 3, 2004, pp. 395–409. https://doi.org/https://doi.org/10.1155/2004/523692.

[33] Géradin, M., and Rixen, D., *Mechanical vibrations: theory and application to structural dynamics*, John Wiley & Sons, 2014.

[34] Clark, R. L., "Accounting for Out-of-bandwidth Modes in the Assumed Modes Approach: Implications on Colocated Output Feedback Control," *Journal of Dynamic Systems, Measurement and Control, Transactions of the ASME*, Vol. 119, No. 3, 1997, pp. 390–395. https://doi.org/10.1115/1.2801270.

[35] Dossogne, T., Noël, J. P., Masset, L., Kerschen, G., and Peeters, B., "Understanding and Modeling Nonlinear Behaviors in Aerospace Structures using Sine-Sweep Testing," *Aerospace Lab*, , No. 14, 2018, pp. 1–15.

[36] Masri, S. F., and Caughey, T. K., "A Nonparametric Identification Technique for Nonlinear Dynamic Problems," *Journal of Applied Mechanics*, Vol. 46, No. 2, 1979, pp. 433–447. https://doi.org/10.1115/1.3424568.

[37] Volvert, M., and Kerschen, G., "Phase Resonance Nonlinear Modes of Mechanical Systems," *Journal of Sound and Vibration*, Vol. 511, 2021, p. 116355. https://doi.org/https://doi.org/10.1016/j.jsv.2021.116355.

[38] Abeloos, G., "Control-Based Methods for the Identification of Nonlinear Structures," *PhD thesis*, University of Liège, 2022. https://doi.org/https://hdl.handle.net/2268/295414.